The Astrophysical Journal, 807:33 (10pp), 2015 July 1 doi:10.1088/0004-637X/807/1/33

A PROPELLER MODEL FOR THE SUB-LUMINOUS STATE OF THE TRANSITIONAL MILLISECOND PULSAR PSR J1023+0038

A. Papitto[1] and D. F. Torres[1,2]
[1] Institute of Space Sciences (CSIC-IEEC), Campus UAB, Carrer de Can Magrans, S/N, E-08193, Cerdanyola del Vallés, Barcelona, Spain
[2] Institució Catalana de Recerca i Estudis Avançats (ICREA), E-08010 Barcelona, Spain
Received 2014 November 17; accepted 2015 April 17; published 2015 June 26

ABSTRACT

The discovery of millisecond pulsars switching between states powered either by the rotation of their magnetic field or by the accretion of matter has recently proved the tight link shared by millisecond radio pulsars and neutron stars in low-mass X-ray binaries. Transitional millisecond pulsars also show an enigmatic intermediate state in which the neutron star is surrounded by an accretion disk and emits coherent X-ray pulsations, but is sub-luminous in X-rays with respect to accreting neutron stars, and is brighter in gamma-rays than millisecond pulsars in the rotation-powered state. Here, we model the X-ray and gamma-ray emission observed from PSR J1023+0038 in such a state based on the assumptions that most of the disk in-flow is propelled away by the rapidly rotating neutron star magnetosphere, and that electrons can be accelerated to energies of a few GeV at the turbulent disk–magnetosphere boundary. We show that the synchrotron and self-synchrotron Compton emission coming from such a region, together with the hard disk emission typical of low states of accreting compact objects, is able to explain the radiation observed in the X-ray and gamma-ray bands. The average emission observed from PSR J1023+0038 is modeled by a disk in-flow with a rate of $1–3\times10^{-11}\,M_{\odot}\,\mathrm{yr}^{-1}$, truncated at a radius ranging between 30 and 45 km, compatible with the hypothesis of a propelling magnetosphere. We compare the results we obtained with models that assume that a rotation-powered pulsar is turned on, showing how the spin-down power released in similar scenarios is hardly able to account for the magnitude of the observed emission.

Key words: accretion, accretion disks – gamma rays: stars – magnetic fields – pulsars: individual (PSR J1023+0038)

1. INTRODUCTION

Millisecond pulsars are neutron stars (NSs) that attained their quick rotation during a Gyr-long phase of accretion of matter transferred from a companion star in a low-mass X-ray binary (LMXB; Bisnovatyi-Kogan & Komberg 1974; Alpar et al. 1982; Radhakrishnan & Srinivasan 1982; Wijnands & van der Klis 1998). At the end of such an X-ray bright phase, a pulsar powered by the rotation of its magnetic field turns on, driving pulsed emission from the radio to the gamma-ray energy band. The recent discovery of IGR J18245−2452, a pulsar observed to swing between an accretion- (X-ray) and a rotation-powered (radio) pulsar regime, proved the tight evolutionary link existing between these two classes of systems (Papitto et al. 2013). IGR J18245−2452 turned on in 2013 March as an X-ray bright ($L_X \gtrsim 10^{36}\,\mathrm{erg\,s^{-1}}$), accreting millisecond pulsar in the globular cluster M28; cross-referencing with catalogs of radio pulsars we realized that the source behaved as a rotation-powered radio pulsar a few years before. A few days after the end of the two-week X-ray outburst, the source reactivated as a radio pulsar. Variations of the mass in-flow rate toward the NS are able to drive such state transitions. During the rotation-powered regime, the pressure of the pulsar ejects the matter transferred from the companion star, causing irregular eclipses of the radio pulsed emission. Occasionally, the pressure of the matter transferred from the companion overcomes the pulsar pressure and yields the formation of an accretion disk around the NS.

The state transitions observed from two more pulsars, PSR J1023+0038 (Archibald et al. 2009; Patruno et al. 2014; Stappers et al. 2014) and XSS J12270−4859 (Bassa et al. 2014; Bogdanov et al. 2014; Roy et al. 2014), as well as in archival observations of IGR J18245−2452 (Papitto et al. 2013; Pallanca et al. 2013; Linares et al. 2014), showed that the presence of an accretion disk does not necessarily imply the onset of a bright X-ray outburst. These three *transitional* millisecond pulsars showed an intermediate regime, which we dub a *sub-luminous* disk state, whose main features are the following.

1. The presence of an accretion disk, as indicated by Hα broad, sometimes double-peaked emission lines observed in the optical spectrum (Wang et al. 2009; Halpern et al. 2013; Pallanca et al. 2013; de Martino et al. 2014).
2. An average X-ray luminosity ranging from 10^{33} to $10^{34}\,\mathrm{erg\,s^{-1}}$, intermediate between the level observed at the peak of the X-ray outbursts ($10^{36}\,\mathrm{erg\,s^{-1}}$) and during the rotation-powered emission ($<10^{32}\,\mathrm{erg\,s^{-1}}$); the X-ray emission is variable on timescales of a few tens of seconds and has a spectrum described by a power law with index $\Gamma \simeq 1.5$ and no cutoff below 100 keV (Saitou et al. 2009, De Martino et al. 2010, 2013,Papitto et al. 2013; Linares et al. 2014; Patruno et al. 2014; Tendulkar et al. 2014). So far, IGR J18245−2452 is the only *transitional* millisecond pulsar that has also been observed into an X-ray bright ($L_X \gtrsim 10^{36}\,\mathrm{erg\,s^{-1}}$) outburst.
3. The presence of accretion-driven X-ray coherent pulsations at an rms amplitude between 5% and 10%, which were detected from the two sources, PSR J1023+0038 (Archibald et al. 2014) and XSS J12270−4859 (Papitto et al. 2014), that were observed at a high enough temporal resolution during the *sub-luminous* disk state. A search for radio pulsations was conducted in the case of PSR J1023+0038, but none were detected with an upper limit on the pulsed flux that was one order of magnitude lower than during the

rotation-powered state (Bogdanov et al. 2014; Stappers et al. 2014).

4. Correlated variability of the X-ray and ultraviolet emission on timescales of hundreds of seconds (De Martino et al. 2013).
5. A 0.1–10 GeV gamma-ray luminosity of $\approx 10^{34}$ erg s^{-1} detected from the two *transitional* millisecond pulsars of the Galactic field, PSR J1023+0038 and XSS J12270−4859[3], up to ten times brighter with respect to the levels observed during the rotation-powered state (de Martino et al. 2010; Hill et al. 2011, Papitto et al. 2014, Stappers et al. 2014; Takata et al. 2014). Candidate transitional millisecond pulsars have been also recently proposed to explain the otherwise unidentified gamma-ray sources 1FGL J0523.5−2529 (Strader et al. 2014) and 3FGL J1544.6−1125 (Bogdanov & Halpern 2015). *Transitional* pulsars are the only low-mass X-ray binaries from which gamma-ray emission has been detected so far by *Fermi*/LAT (see Section 5.2 for a discussion of possible selection effects).
6. Bright, flat-spectrum radio emission indicative of partially absorbed synchrotron emission; transitional millisecond pulsars in this state are 1–2 orders of magnitude brighter at radio frequencies with respect to the extrapolation of the radio/X-ray correlation observed from X-ray brighter NSs (Deller et al. 2014).

X-ray flaring around a luminosity of about 10^{33}–10^{34} erg s^{-1}, lasting from a few days to a few months, has also been reported for a number of LMXBs hosting an NS (Aql X-1, Rutledge et al. 2001; Campana & Stella 2003; Cackett et al. 2011; Degenaar & Wijnands 2012; Bernardini et al. 2013; Cen X-4, EXO 1745−248, SAX J1750.8−2900, Wijnands & Degenaar 2013; Coti Zelati et al. 2014; XMM J174457−2850.3, Degenaar et al. 2014). These observations suggest that an intermediate state between outburst and quiescence is also realized in sources that so far have not shown signs of a magnetosphere.[4] However, the presence of a spectral cutoff at about 10 keV in the spectrum of Cen X-4 (Chakrabarty et al. 2014) and the lack of a detection at gamma-ray energies indicate that in some of these systems different radiation processes might be at work with respect to *transitional* millisecond pulsars in the *sub-luminous* disk state.

The observation of coherent X-ray pulsations from PSR J1023+0038 and XSS J12270−4859 during the disk state is most easily explained in terms of the channelling of at least part of the disk mass in-flow onto the magnetic poles (see Archibald et al. 2014; Papitto et al. 2014; and Section 5 below). For this to happen, the disk should penetrate into the light cylinder of the pulsar, ruling out the possibility that a rotation-powered pulsar is turned on. However, the exact nature of the energy reservoir that powers the emission of *transitional* millisecond pulsars in the *sub-luminous* disk state is still uncertain, as well as the mechanism that accelerates charges to relativistic energies and yields the observed gamma-ray emission. Papitto et al. (2014, P14 in the following; see also Bednarek 2009) proposed that a millisecond pulsar that prevents most of the mass in-flow from accreting onto the NS surface due to its rapid rotation (i.e., the propeller effect, Illarionov & Sunyaev 1975) could accelerate electrons at the boundary between the disk and the propelling magnetosphere. If this happens, P14 showed that the synchrotron emission yielded by the interaction of electrons with the field lines at the magnetospheric boundary makes a significant contribution to the X-ray observed emission, and that gamma-rays are produced by Compton up-scattering of the synchrotron photons. Here we apply this model to explain the X-ray/gamma-ray emission observed from PSR J1023+0038 after its state transition to the *sub-luminous* disk state in 2013 June (Patruno et al. 2014; Stappers et al. 2014), explicitly taking into account the detection of coherent pulsations in the X-ray light curve. PSR J1023+0038 is particularly suited for the study of the *sub-luminous* disk state, as parameters such as distance, spin period, and magnetic dipole moments are known within a high accuracy.

2. PSR J1023+0038

PSR J1023+0038 was discovered in 2007 as a 1.7 millisecond radio pulsar in a 4.8 hr orbit around a 0.2 $M_\odot$ companion star (Archibald et al. 2009). Observation of double-peaked emission lines in its optical spectrum indicated that in 2001 it likely had an accretion disk (Wang et al. 2009), suggesting that a state transition must have occurred between then and 2007. The upper limit on the X-ray luminosity when a disk was present (2.7×10^{34} erg s^{-1} for a distance of 1.37 kpc, Deller et al. 2012) led Archibald et al. (2009) to assume that mass infall was halted before reaching the NS surface by the propeller inhibition of accretion.

During the radio pulsar state PSR J1023+0038 showed a spin-down luminosity of $L_{\rm sd} = 4.4 \times 10^{34}$ erg s^{-1} (Archibald et al. 2013). Using the relation given by Spitkovsky (2006), the magnetic dipole is estimated as $\mu = 0.79 \times 10^{26}\ (1 + \sin^2 \alpha)^{-1}$ G cm^3, where α is the angle between the magnetic and spin axes. In the radio pulsar state, the X-ray emission is described by a power law with index $\Gamma = 1.17(8)$ and a 3–79 keV luminosity of $7.4(4) \times 10^{32}$ erg s^{-1} (Tendulkar et al. 2014; see also Bogdanov et al. 2011), and the gamma-ray emission by a log-parabola with $\beta = 2.49(3)$ and 0.1–100 GeV luminosity of $1.2(2) \times 10^{33}$ erg s^{-1} (Nolan et al. 2012). The efficiency of spin-down luminosity conversion in the considered bands is 1.7% and 2.7%, respectively.

In 2013 June the disappearance of radio pulsations at all orbital phases (Stappers et al. 2014) and the appearance of double-peaked Hα emission lines in the optical spectrum (Halpern et al. 2013) marked a transition to an accretion, X-ray *sub-luminous* disk state. The X-ray luminosity increased by one order of magnitude with respect to the level shown in the radio pulsar state (Patruno et al. 2014). Tendulkar et al. (2014) modeled with a power law with index $\Gamma = 1.66(6)$ the spectra observed in the disk state by the *Swift* X-ray telescope and by *NuStar* in the 0.3–10 and 3–79 keV energy bands, respectively (the orange strip in Figure 1). The 3–79 keV luminosity was estimated as $5.8(2) \times 10^{33}$ erg s^{-1}, which corresponds to a luminosity of 7.3×10^{33} erg s^{-1} in the 0.3–79 keV band, i.e., 16.6% of the spin-down power.

During the *sub-luminous* disk state, three flux modes are observed both in soft (Bogdanov et al. 2014; Patruno et al. 2014) and in hard X-rays (Tendulkar et al. 2014). On the one hand, a low and a high state are characterized by a flux change of one order of magnitude. On the other hand, the source occasionally presents an even brighter flaring state. Coherent

[3] Gamma-ray emission from the globular cluster hosting IGR J18245−2452, M28, has been detected by *Fermi*/LAT, but source confusion does not allow us to pinpoint its origin in the cluster.

[4] Aql X-1 showed accretion-powered coherent pulsations only during a brief 150 s interval (Casella et al. 2008).

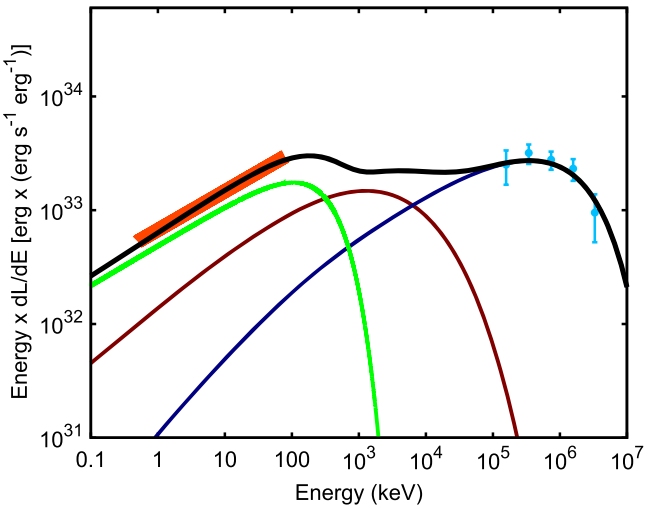

Figure 1. Average SED observed from PSR J1023+0038 in X-rays (orange strip, from Tendulkar et al. 2014) and gamma-rays (cyan points, from Takata et al. 2014), evaluated for a distance of 1.37 kpc. The total SED evaluated with our modeling for $\xi = 0.15$ (i.e., 15% of the advected disk energy available to power the propeller emission), $\beta = 0$ (anelastic propeller collision), $k_{\rm ej} = 0.99$ (i.e., 99% of disk mass ejected), and $\omega_* = 2.5$ is plotted as a black solid line. Synchrotron, SSC, and accretion flow (i.e., the sum of disk and NS emission) components are plotted as red, blue, and green lines, respectively.

pulsations were detected at an rms amplitude of $\simeq$6% when the source is in the high state, in which it spends 70% of the time (Archibald et al. 2014). PSR J1023+0038 also brightened in gamma-rays, attaining a 0.1–100 GeV luminosity of $(9.6 \pm 1.3) \times 10^{33}$ erg s^{-1}, i.e., 22% of the spin-down power (Takata et al. 2014). The average *Fermi*/LAT spectrum is described by a power law with index 1.8(2), cutoff at an energy of 2.3(9) GeV (cyan points in Figure 1, taken from Figure 2 of Takata et al. 2014).

3. THE MODEL

According to the standard theory of disk accretion onto a magnetized rotator, three regimes are realized depending on the radius $R_{\rm in}$ at which the disk is truncated by the rotating magnetosphere (see Lipunov 1987 for a review). If $R_{\rm in}$ is larger than the light-cylinder radius,

$$R_{\rm lc} = cP/2\pi, \tag{1}$$

where P is the spin period of the NS, the pulsar emits a relativistic wind of particles and magneto-dipole radiation that overcomes the gravitational force on the plasma transferred from the companion star (the *ejector* state). As the pulsar pressure declines with the distance from the NS less steeply than the disk pressure, the emission of a pulsar in such a state is expected to disrupt the entire disk flow (Shvartsman 1970; Burderi et al. 2001), even if stable solutions implying the survival of the disk for $R_{\rm in} \sim$ few $R_{\rm lc}$ have been shown by Ekşi & Alpar (2005).

At a larger mass in-flow rate the in-falling plasma manages to penetrate into the light cylinder and suppresses the relativistic wind of particles and the rotation-powered pulsed emission. Accretion onto the NS surface can take place freely only if the plasma in the disk rotates faster than the NS magnetic field at the inner disk boundaries, i.e., if $R_{\rm in}$ is smaller than the corotation radius,

$$R_c = \left(GMP^2/4\pi^2\right)^{1/3}, \tag{2}$$

where M is the NS mass and Keplerian rotation is assumed for disk plasma. Otherwise, if $R_{\rm lc} > R_{\rm in} > R_c$, the accretion flow is repulsed by the quickly rotating magnetosphere and can be ejected from the system, i.e., the system is assumed to be in the propeller state (Illarionov & Sunyaev 1975).

A useful parameterization of the problem is obtained by introducing the dimensionless fastness,

$$\omega_* \equiv \frac{\Omega_*}{\Omega_K\left(R_{\rm in}\right)} = \left(\frac{R_{\rm in}}{R_c}\right)^{3/2} \tag{3}$$

(Ghosh et al. 1977) where Ω_K is the Keplerian angular frequency and Ω_* is the NS angular frequency. For values of ω_* ranging between 1 and 1.26, not enough kinetic energy is given to plasma to eject it from the system; matter is then expected to accumulate in the disk and eventually overcome the pressure barrier set by the magnetosphere, leading to a burst of accretion (Spruit & Taam 1993; D'Angelo & Spruit 2010). Larger values of ω_* ranging between 1.3 and 2.5 have been considered by Lii et al. (2014) to perform axisymmetric magneto-hydrodynamical simulations of accretion onto a rapidly rotating magnetized star, driven by magneto-rotational instability. While they also observed cycles between matter accumulation at the inner disk boundary and episodes of accretion onto the star, they found that part of the in-flow was ejected by the quickly rotating magnetosphere. The fraction of the matter actually ejected by the system with respect to what was accreted was found to increase continuously with ω_*.

The determination of an analytical relation for $R_{\rm in}$ as a function of the main physical quantities characterizing such systems (such as the disk mass in-flow rate $\dot{M}_d$, the magnetic moment μ, the mass M_*, and the spin period P of the magnetized rotator), and of the physics of the field-disk interaction, is one of the open problems of the current theoretical investigation in the field (see, e.g., Ghosh & Lamb 1979; Wang 1996; Bozzo et al. 2009). Usually, the inner disk radius is expressed as a fraction k_m of the Alfvén radius $R_{\rm A}$, a scale size obtained by equating the inward pressure of an assumed spherical in-flow to the outward pressure of a dipolar magnetosphere

$$R_{\rm in} = k_m R_{\rm A} = k_m \left[\frac{\mu^4}{2GM_*\dot{M}_d^2}\right]^{1/7}. \tag{4}$$

Values of k_m ranging from 0.5 to 1 have been proposed by a number of authors, depending on the details of the physics of the disk–magnetosphere interactions (see Ghosh 2007, and references therein). In 3D MHD simulations of disk accretion around a fast rotator Lii et al. (2014) found that a value of $k_m = 0.7$ matched the disk truncation radius reproduced by their modeling.

Assuming that the coherent X-ray pulsations observed from PSR J1023+0038 in the disk state were due to an accretion of matter onto a fraction of the NS surface, we can estimate an upper and a lower limit on the mass accretion rate onto the NS. The latter, $\dot{M}_{\rm NS}$, is constrained, assuming that either the whole

observed X-ray luminosity or just the pulsed luminosity is due to accretion onto the NS. Considering that $L_X(0.3-79\,\mathrm{keV}) = 7.3\times10^{33}\,\mathrm{erg\,s^{-1}}$ we then obtain

$$\begin{aligned} 5\times10^{-14}M_\odot\ \mathrm{yr}^{-1} &\simeq \left(\sqrt{2}A_{\rm rms}\right)\frac{L_X R_{\rm NS}}{GM_{\rm NS}} \\ &< \dot{M}_{\rm NS} < \\ \frac{L_X R_{\rm NS}}{GM_{\rm NS}} &\simeq 6\times10^{-13}M_\odot\ \mathrm{yr}^{-1}, \end{aligned} \quad (5)$$

where $A_{\rm rms}\simeq 0.06$ is the rms amplitude of X-ray pulsations (Archibald et al. 2014), and we assume an NS mass of 1.4 $M_\odot$ and a radius of 10 km, as throughout the paper, and an efficiency of conversion of accretion power into observed X-rays of unity. Given a magnetic moment of $\mu = 0.79\times10^{26}\,\mathrm{G\,cm^3}$ (see Archibald et al. 2013, and Section 2) and $k_m = 0.7$ (Lii et al. 2014), in order to keep the inner disk radius within a few times the corotation radius (23.8 km for PSR J1023+0038, Archibald et al. 2009), Equation (4) indicates that the disk mass accretion rate must be

$$\dot{M}_d \simeq 7\times10^{-11}\,M_\odot\ \mathrm{yr}^{-1} > 100\times\dot{M}_{\rm NS}. \quad (6)$$

By interpreting X-ray pulsations as due to accretion onto the NS magnetic poles, and assuming the inner disk radius can be reproduced by a relation like Equation (4), it then follows that $\gtrsim$99% of the matter in-flowing in the disk must be ejected from the inner disk boundary for mass conservation to hold.

In P14 we developed a model to interpret the emission of millisecond transitional pulsars in the sub-luminous disk state assuming the following.

1. Accretion onto the NS surface is inhibited by the propeller effect (i.e., $R_{\rm lc} > R_{\rm in} > R_c$).
2. Electrons are accelerated to relativistic energies at the turbulent boundary between the disk and the propelling magnetosphere.
3. Relativistic electrons interact with the NS magnetic field lines producing synchrotron emission that explains (at least part of) the X-ray emission.
4. Synchrotron photons are up-scattered by relativistic electrons to explain the emission observed in the gamma-ray band.

Here, we apply a similar model to the case of PSR J1023+0038, restricting to a range of values of fastness ranging from 1.5 to 2.5 in order for the inner disk radius to be close enough to the corotation radius to let a fraction of matter effectively accrete down to the NS surface, as observed.

3.1. The Energy Budget

Energy conservation dictates that the energy available to power the radiative emission from the disk ($L_{\rm disk}$), the inner disk boundary ($L_{\rm prop}$), and the NS surface ($L_{\rm NS}$), as well as the kinetic energy of the outflow launched by a propelling NS ($\dot{M}_{\rm ej}v_{\rm out}^2/2$) and the energy converted in internal energy of the flow and advected ($\dot{E}_{\rm adv}$), should be equal to the sum of the gravitational energy liberated by the infall of matter $\dot{E}_g$, and the energy released by the NS magnetosphere through the torque N applied at the inner disk radius

$$L_{\rm prop} + L_d + \dot{E}_{\rm adv} + L_{\rm NS} + \frac{1}{2}\dot{M}_{\rm ej}v_{\rm out}^2 = \dot{E}_g + N\Omega_*, \quad (7)$$

where $\Omega_* = 2\pi/P$ is, as before, the NS angular velocity. In a stationary state, mass conservation is expressed by:

$$\dot{M}_d = \dot{M}_{\rm NS} + \dot{M}_{\rm ej}. \quad (8)$$

We define the fraction of mass ejected as

$$k_{\rm ej} = \frac{\dot{M}_{\rm ej}}{\dot{M}_d} = 1 - \frac{\dot{M}_{\rm NS}}{\dot{M}_d}. \quad (9)$$

Considering the reasoning developed in the previous section, we consider values $k_{\rm ej} > 0.95$ for the case of PSR J1023+0038. According to these definitions, the gravitational energy liberated by the mass infall is:

$$\dot{E}_g = \frac{GM\dot{M}_d}{R_{\rm in}} + GM\dot{M}_{\rm NS}\left(\frac{1}{R_{\rm NS}} - \frac{1}{R_{\rm in}}\right). \quad (10)$$

We assume that the NS luminosity is given by efficient conversion of the infalling gravitational energy, so that

$$L_{\rm NS} = GM\dot{M}_{\rm NS}\left(\frac{1}{R_{\rm NS}} - \frac{1}{R_{\rm in}}\right). \quad (11)$$

Furthermore, we express the disk luminosity as a fraction η of the energy radiated by an optically thick, geometrically thin disk

$$L_d = \eta\frac{GM\dot{M}_d}{2R_{\rm in}}. \quad (12)$$

The case of a radiatively efficient disk is realized for $\eta = 1$. For values of η lower than unity, we assume that the energy that is not radiated by the disk is partly advected, and partly made available to power the propeller emission. To express the latter, we introduce a parameter, ξ, that will represent the fraction of gravitational energy that is liberated in the disk and can be used to power the propeller emission; for $\xi = 0$ no such energy is used, while for $\xi = 1-\eta$, all the disk energy that is not radiated is converted into propeller luminosity. This implicitly means that we express

$$\dot{E}_{\rm adv} = (1-\eta-\xi)\frac{GM\dot{M}_d}{2R_{\rm in}}. \quad (13)$$

Substituting the previous formulae in Equation (7), we obtain an expression for the energy that can be radiated from the disk–magnetospheric boundary:

$$L_{\rm prop} = \left(\frac{1+\xi}{2}\right)\frac{GM\dot{M}_d}{R_{\rm in}} + N\Omega_* - \frac{1}{2}k_{\rm ej}\dot{M}_d v_{\rm out}^2. \quad (14)$$

Similarly, the conservation of angular momentum at the inner disk boundary yields:

$$\dot{M}_{\rm ej}R_{\rm in}v_{\rm out} = N + \dot{M}_d\Omega_K R_{\rm in}^2. \quad (15)$$

The left-hand side represents the angular momentum imparted to eject matter, while the right-hand side represents the torque exerted by the NS magnetosphere and the angular momentum advected by disk matter in Keplerian rotation appear. In order

to express the velocity of the outflow $v_{\rm out}$ we follow Ekşi et al. (2005), who treated the interaction at the inner disk boundary as a collision of particles, obtaining

$$v_{\rm out} = \Omega_K(R_{\rm in})R_{\rm in}\left[\omega_*(1+\beta)-\beta\right], \quad (16)$$

where the elasticity parameter β has been introduced. The case of completely anelastic collision is given by $\beta = 0$, while the totally elastic case is described by $\beta = 1$. Inserting the expression for the outflow velocity (Equation (16)) into Equations (14) and (15), and solving for $L_{\rm prop}$ and N gives

$$L_{\rm prop} = \frac{GM\dot{M}_d}{R_{\rm in}}\left\{\frac{1+\xi}{2} - \omega_* + k_{\rm ej}\right.$$
$$\left.\left[\omega_*\left[\omega_*(1+\beta)-\beta\right] - \frac{1}{2}\left[\omega_*(1+\beta)-\beta\right]^2\right]\right\}$$
$$N = \dot{M}_d\sqrt{GMR_{\rm in}}\left\{k_{\rm ej}\left[\omega_*(1+\beta)-\beta\right]-1\right\}. \quad (17)$$

If most of the in-flowing matter is ejected from the inner disk boundary ($k_{\rm ej} \simeq 1$), the equation for the propeller luminosity simplifies to

$$L_{\rm prop} = \frac{GM\dot{M}_d}{2R_{\rm in}}\left[\xi + \left(\omega_*-1\right)^2\left(1-\beta^2\right)\right]. \quad (18)$$

We can immediately note that if the energy advected in the disk is not available to power the propeller ($\xi = 0$) and the propeller collision is completely elastic ($\beta = 1$), all the available energy goes into powering the kinetic energy of the outflow, and the propeller luminosity vanishes. On the other hand, if the collision is completely anelastic ($\beta = 0$), the outflow velocity equals the velocity of the magnetosphere at the inner disk radius, and the propeller luminosity is maximized. In what follows, we only consider the latter case. Using Equation (4) to relate the disk mass accretion rate to the inner disk radius and Equation (3) to express the latter in terms of the corotation radius and the fastness, we obtain for the parameters of PSR J1023+0038

$$L_{\rm prop} = 1.75\times10^{35}\,\omega_*^{-3}\left[\xi + \left(\omega_*-1\right)^2\right.$$
$$\left.\times\left(1-\beta^2\right)\right]\,{\rm erg\ s^{-1}}. \quad (19)$$

This relation is plotted in Figure 2 for $\beta = 0$ and ξ equal to 0 (i.e., no disk gravitational energy available to power the propeller emission, red solid line), and 0.15 (red dashed line). Green and blue lines in the same figure represent the cases $k_{\rm ej} = 0.99$ and 0.95, respectively. Values of the propeller luminosity of few $\times10^{34}\,{\rm erg\ s^{-1}}$ are obtained for a fastness $\gtrsim$1.5.

3.2. The Electron Population

Like in P14, we assume that at the inner disk boundary the propelling magnetosphere is able to accelerate electrons to relativistic energies. To simplify, the electron energy distribution is assumed to be described by a power law with an exponential cutoff:

$$\frac{dN_e}{d\gamma} = N_0\gamma^{-\alpha}\exp\left(-\frac{\gamma}{\gamma_{\rm max}}\right). \quad (20)$$

These electrons produce synchrotron emission by interacting with the magnetic field at the disk–magnetosphere interface

$$\bar{B} = \frac{\mu}{R_{\rm in}^3} = \frac{\mu}{R_c^3\omega_*^2}. \quad (21)$$

At high energies the synchrotron emission is cut off at $E_{\rm syn} \simeq 10(\bar{B}/10^6\ {\rm G})\,(\gamma_{\rm max}/10^4)^2\,{\rm MeV}$, while at low energies the emission is self-absorbed below a few eVs (see Papitto et al. 2014 and references therein). We further assume that the electron distribution lies in a region of volume V (giving an electron density $n_e = N_0/V$), and up-scatters the synchrotron photons up to an energy $E_{\rm ssc} = \gamma_{\rm max}m_ec^2 \simeq 5(\gamma_{\rm max}/10^4)\,{\rm GeV}$, to give a self-synchrotron Compton (SSC) component. Therefore, in our model, the X-ray emission is given by the sum of two components: the synchrotron emission powered by the propeller luminosity $L_{\rm prop}$, and the X-rays produced by the accretion flow, either from the disk, the NS surface, or a corona surrounding the system. On the other hand, the gamma-ray emission falling in the 0.1–10 GeV range could only arise as the SSC component of the propeller emission.

The parameters of the electron distribution (α, $\gamma_{\rm max}$, n_e) and the volume V of the region of acceleration can be then adjusted such that:

(i) they model the gamma-ray emission as the self-synchrotron Compton component of the same electron population that produces a good part of the X-ray emission; and

(ii) for a fixed value of the fastness ω_*, they give a total propeller luminosity (i.e, the sum of synchrotron and self-synchrotron Compton contributions) that matches the value given above by Equation (17).

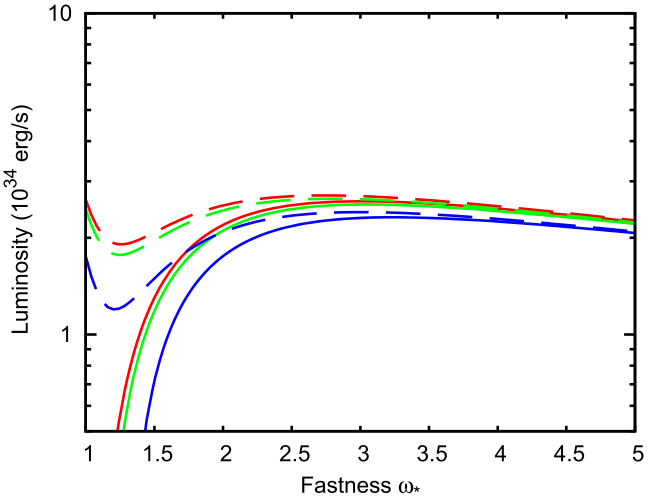

Figure 2. Propeller luminosity in the case of almost total ejection ($k_{\rm ej} = 1$) for $\xi = 0$ (i.e., no disk gravitational energy available to power the propeller emission, red solid line) and 0.15 (red dashed line). The green solid and dashed lines refer to the case $k_{\rm ej} = 0.99$ evaluated for $\xi = 0$ and 0.15, respectively. The blue solid and dashed lines refer to the case $k_{\rm ej} = 0.95$ evaluated for $\xi = 0$ and 0.15, respectively. All the curves are plotted for a totally anelastic interaction ($\beta = 0$).

As the X-ray emission is given by the sum of the contribution of the propeller and the accretion flow luminosity in that energy range, and no cutoff is observed from 0.5 to 80 keV, we cannot disentangle the relative weight of these components. At low luminosities ($\lesssim 10^{34}$–10^{35} erg s^{-1}), the X-ray spectrum of the accretion flow onto compact objects is generally dominated by a power law with index Γ between 1.5 and 2.5, extending to high energies ($\gtrsim$100 keV; see, e.g., Reynolds et al. 2010, Armas Padilla et al. 2013a, 2013b). A similar spectral shape is also observed for the pulsed emission of accreting millisecond pulsars (see Patruno & Watts 2012 and references therein). We then describe the contribution of the accretion flow in the X-ray band as a power law with index $\Gamma = 1.65$, cut off at an energy outside the observed energy band (we arbitrarily chose 300 keV as an example), that, summed to the synchrotron and SSC component, gives an 0.3–79 keV X-ray flux equal to the one observed in that energy band. Then, we require that once the propeller contribution to the X-ray emission is fixed by our modeling of the gamma-rays, the accretion flow X-ray emission does not exceed the observed emission. A lower limit on the contribution of the accretion flow to the X-ray flux is given by the pulsed flux amplitude, $\sqrt{2} A_{\rm rms} L_X \simeq 6 \times 10^{32}$ erg s^{-1}, while an upper limit to the accretion flow X-ray luminosity is given by the total luminosity observed in that band (7.3×10^{33} erg s^{-1}).

4. RESULTS

To simulate the emission processes that take place in a magnetized environment filled by a relativistic population of electrons we used the codes described by Torres (2004), de Cea del Pozo et al. (2009), and Martín et al. (2012). The cutoff observed at a few GeVs in the *Fermi/LAT* energy band requires a maximum electron energy of $\gamma_{\rm max} = 10^4$. We also set the index of the electron distribution as $\alpha = 2$.

In order to have enough energy to power the propeller emission necessary to explain the observed gamma-ray emission, we fixed the elasticity parameter to 0 (i.e., inelastic scattering), allowed for 15% of the energy advected in the disk to be used to power the propeller emission (i.e., $\xi = 0.15$), and set $k_{\rm ej} = 0.99$ (i.e., only 1% of the disk mass is accreted onto the NS, while the rest is ejected). This gives a maximum propeller luminosity of $\gtrsim 2.5 \times 10^{34}$ erg s^{-1} for values of the fastness between 1.5 and 2.5 (see Figure 2). We modeled the spectral energy distribution (SED) considering different values of the fastness in this range.

As the corotation radius and the dipole magnetic moment of PSR J1023+0038 are measured the inner disk radius, the strength of the magnetic field at the disk inner boundary, and the disk mass accretion rate are fixed by the choice of ω_* (see Equations (3), (4), and (21), respectively). For a given value of ω_*, we then evaluate the electron density n_e and the volume V of the acceleration region requested to describe the observed gamma-ray spectrum with the SSC component (which requires a luminosity of $L_{\rm SSC} \simeq 1.7 \times 10^{34}$ erg s^{-1}), and to give a total propeller luminosity equal to the value given by Equation (17) when $L_{\rm SSC}$ is summed to the synchrotron component. The values of the parameters obtained for different values of ω_* are listed in Table 1, while the SED obtained for $\omega_* = 2.5$ is plotted in Figure 2, as an example. The X-ray luminosity attributed to the accretion flow, $L^X_{\rm accr}$, is evaluated as the difference between the luminosity observed in the 0.3–79 keV band (7.3×10^{33} erg s^{-1}) and the sum of the synchrotron and SSC luminosity falling in the same energy band.

For values of ω_* close to 1.5, the propeller luminosity is lower, and in order to explain the observed SED with our modeling, a large electron density and a very small volume of emission of the SSC component are required, corresponding to a typical size of the emission region of $\approx$0.05 km. Increasing ω_*, a larger region with typical size of $\lesssim$1 km is instead allowed. We further discuss this below.

We checked that the assumption that only 1% of the disk mass is accreted is compatible with the parameters of our modeling by evaluating the ratio between the NS mass accretion rate (constrained by using Equation (5)), and the values of the disk mass accretion rate listed in Table 1. For all the models listed in Table 1 this yielded values of k_{ej} ranging between 0.94 and 0.998, thus compatible with the assumed value of 0.99.

The efficiency of conversion of gravitational energy into X-rays was estimated as $\eta_X = L^X_{\rm accr}/\dot{E}_g$. Plugging the parameters of our models into Equation (10), we obtain values of the efficiency ranging between $\approx$5% and 20%, with larger efficiency values obtained for the models with a larger fastness. As the X-ray efficiency owing to the in-fall of matter onto the NS surface is unlikely much lower than one, we conclude that the accretion disk efficiency must be lower than 20% (note that according to our definitions, the efficiency of a geometrically thin, optically thick disk that emits all of its energy in X-rays, is $\eta = 0.5$).

4.1. A Comparison with XSS J12270−4859

The generic idea behind the model used here to interpret the emission observed from PSR J1023+0038 in the *sub-luminous* disk state has been previously successfully applied to the emission of XSS J12270−4859 in the same state (P14). However, in that paper it was assumed that all of the gravitational energy given off by the matter in-flow was available to power the propeller emission and outflow, and consequently, the interplay between the disk and the propeller luminosities was not explored as done above. Considering the formalism developed in Section 3, that assumption corresponds to the case $\eta = 0$ and $\xi = 1$. This case is extreme and probably unlikely, since it would require an X-ray *dark* accretion flow.

However, the similarities between the average SED observed from these two sources, and the results obtained in the case of PSR J1023+0038 (see Section 4), indicate that our modeling also works in the case of XSS J12270−4859. This is emphasized in Figure 3, where the high-energy SED of XSS J12270−4859 is overplotted as a yellow stripe on the SED of PSR J1023+0038. A distance of 1.4 kpc was considered, equal to the value indicated by the dispersion measure of the radio pulsed signal observed by Roy et al. (2014), and at the lower bound of the 1.4–3.6 kpc range determined by De Martino et al. (2013).

The spin period of XSS J12270−4859 is very similar to that of PSR J1023+0038 ($P = 1.69$ ms), and the magnetic moment can be estimated as $\mu_{26} = 1.13\, I_{45}^{1/2}\, (1 + \sin^2 \alpha)^{-1/2}$ G cm^3 from the observed spin-down rate (Roy et al. 2014). We modeled the SED of XSS J12270−4859 using parameters similar to those used for PSR J1023+0038, and $\omega_* = 2.5$ (see Table 1), obtaining the model that is plotted as a black solid line in Figure 3.

Table 1
Model Parameters used to Model the SED of PSR J1023+0038 and XSS J12270–4859

ξ	k_{ej}	ω_*	R_{in} (km)	$\bar{B}$ (MG)	$\dot{M}$	L_{prop}	n_e (10^{18} cm^{-3})	V (10^{15} cm^3)	L_{ssc}/L_{sync}	L^X_{accr}	η^X_{accr}
PSR J1023+0038											
0.15	0.99	1.50	31.2	2.6	2.7	1.96	54	6×10^{-4}	5.0	0.65	0.06
0.15	0.99	1.75	34.6	1.9	1.9	2.23	10	0.01	2.8	0.59	0.08
0.15	0.99	2.00	37.8	1.5	1.4	2.43	5.0	0.04	2.4	0.55	0.11[a]
0.15	0.99	2.25	40.9	1.15	1.1	2.56	2.1	0.19	2.04	0.51	0.14
0.15	0.99	2.50	43.8	0.94	0.8	2.62	1.3	0.50	1.9	0.48	0.17
XSS J12270–4859											
0.15	0.99	2.50	43.8	1.34	2.4	2.62	1.7	0.21	2.2	0.55	0.08

Note.
[a] Input parameters are listed in the three leftmost columns. Physical quantities obtained using the analytical relations given in the text are listed in columns 4–8. Parameters estimated from the modeling of the observed SED are given in the five rightmost columns. Luminosities are given in units of 10^{34} erg s^{-1}, while the mass in-flow rate is expressed in units of 10^{-11} $M_\odot$ yr^{-1}.

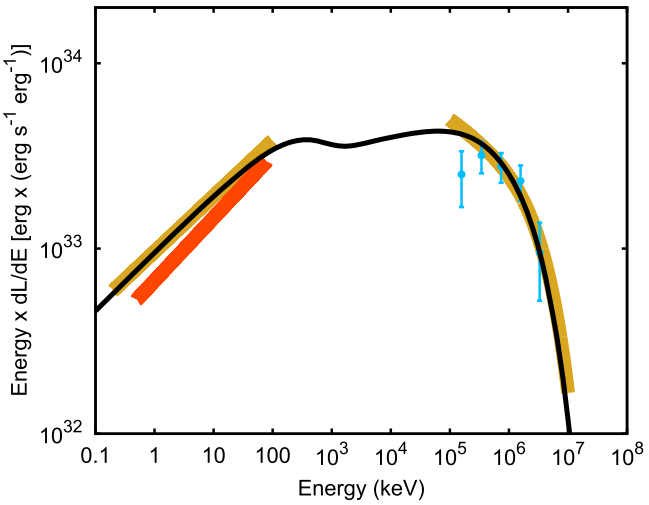

Figure 3. Average SED observed from PSR J1023+0038 (orange stripe and cyan points) and XSS J12270–4859 (yellow stripe; see Papitto et al. (2014) and references therein) for a distance of 1.4 kpc. The model of the XSS J12270–4859 SED, obtained for $\xi = 0.15$, $k_{ej} = 0.99$, and $\omega_* = 2.5$ (see Table 1), is plotted as a black solid line.

5. DISCUSSION

From a theoretical point of view, three possibilities can explain the complex phenomenology of PSR J1023+0038 (and possibly other transitional pulsars) in the *sub-luminous* disk state: a rotation-powered pulsar, accretion onto the NS surface, and a propeller regime. In what follows we discuss these possibilities on the basis of the phenomenology observed.

5.1. Rotation-powered Pulsar Scenario

Coti Zelati et al. (2014), Li et al. (2014), Stappers et al. (2014), and Takata et al. (2014) discussed the phenomenology observed from PSR J1023+0038 in terms of a rotation-powered pulsar active even in the presence of an accretion disk, the radio coherent pulsation being washed out by the enshrouding of the system by intra-binary material. According to these models, the relativistic wind of particles emitted by the pulsar in this state is responsible for the emitted gamma-rays.

Coti Zelati et al. (2014) and Stappers et al. (2014) proposed that the shock between the pulsar wind of particles and the mass in-flow would be the most likely region where the gamma-ray emission is generated, as this would explain the correlation between the observed increase of the gamma-ray emission and the formation of a disk in the system. On the other hand, Li et al. (2014) and Takata et al. (2014) interpreted the gamma-ray emission observed in the *sub-luminous* disk state through inverse Compton scattering of UV disk photons off of the cold pulsar wind. Furthermore, they assumed that the X-rays were due to synchrotron emission taking place in the shock between the pulsar wind and the plasma in-flow. Such a shock would be expected to be stronger in the *sub-luminous* disk state than in the pulsar state, as a larger fraction of the pulsar wind would be intercepted, thus yielding the increased X-ray emission observed.

These ideas are similar to those used for gamma-ray binaries such as LS 5039 or LS I +61 303, where wind and inter-wind shocks are also studied as possible providers of accelerated electrons (e.g., Dubus 2006; Sierpowska-Bartosik & Torres 2008).

The main problematic aspect of applying any rotation-powered scenario to the *sub-luminous disk* state of PSR J1023+0038 is the observation of coherent X-ray pulsations with an rms amplitude of ≈6% during the accretion disk state. Even if X-ray pulsations were also observed during the rotation-powered state, the pulsed 0.5–10 keV X-ray luminosity was 1.2×10^{31} erg s^{-1} (Archibald et al. 2010), roughly one order of magnitude lower than the pulsed luminosity observed during the disk state, 2.5×10^{32} erg s^{-1} (Archibald et al. 2014). Synchronous switching of the radio and X-ray pulsation properties has been observed from rotation-powered pulsars, and interpreted as being due to global changes to the magnetospheric conditions (Hermsen et al. 2013). However, to interpret the X-ray pulsations observed from PSR J1023+0038 in the disk state as rotation-powered, one must admit that when a disk is present, the pulsed flux increases by more than one order of magnitude with respect to the case of an unperturbed magnetosphere. This is contrary to the expectation that high-density plasma from the accretion process shorts out the electric fields that power the electron/positron acceleration in the vacuum gaps, switching off rotation-powered pulsations (see, e.g., Illarionov & Sunyaev 1975). We consider such a scenario highly unlikely. Furthermore, the X-ray pulsations observed from PSR J1023+0038 during the disk state are sinusoidal and have a non-thermal energy distribution (Archibald et al. 2014), whereas

non-thermal X-ray pulsations observed from rotation-powered pulsars are typically narrow-peaked (Zavlin 2007).

In addition to X-ray pulsation, the high conversion efficiency of the spin-down power required to explain the observed radiation also disfavors a rotation-powered scenario. If a radio pulsar is switched on, the spin-down power of 4.4×10^{34} erg s^{-1} is the dominant source of energy for the system; as a matter of fact, for the radio pulsar to be active, the inner disk radius must lie beyond the light-cylinder radius $R_{\rm lc}$ (80.6 km in the case of PSR J1023+0038), and in such a case, the implied mass in-flow rate of less than $\approx 10^{-12}$ $M_\odot$ yr^{-1} (see Equation (4)) would yield an accretion luminosity of $<10^{33}$ erg s^{-1}. The sum of the average luminosity observed from PSR J1023+0038 in the 0.3–79 keV and 0.1–100 GeV energy bands amounts to $\simeq 1.7 \times 10^{34}$ erg s^{-1}, a value that implies a spin-down power conversion efficiency of >40%. A similar value is already larger than the values observed from rotation-powered pulsars, which typically convert 0.1 (Possenti et al. 2002; Vink et al. 2011) and 10% (Abdo et al. 2013) of their spin-down power into observable X-rays and gamma-rays, respectively. In addition, if one considers that the SED is most likely flat (or even peaks) in the 1–10 MeV energy range where observations are not available (see Figure 1 of this paper and Figure 18 of Tendulkar et al. 2014), the total power obtained modeling the SED with two smooth components easily attains a value of the order of the spin-down power or larger (indeed, the power of most of the models listed in Table 1 exceeds such a threshold). Note that a total luminosity significantly exceeding the spin-down power would directly exclude a rotation-powered scenario.

Furthermore, the strong flickering observed in X-rays makes the case for the spin-down power as the lone source of energy even more unlikely. The peak observed X-ray luminosity is of the order of $\approx 2 \times 10^{34}$ erg s^{-1} (Patruno et al. 2014; Tendulkar et al. 2014), i.e., roughly 40% of the spin-down power, alone. No information is available about the correlation between the X-ray and the gamma-ray luminosity on short timescales, but it is clear that unless they are strictly anti-correlated, this likely implies that the limit set by the spin-down power is exceeded at the peak of the flares. Furthermore, the power emitted through synchrotron emission only depends on the acceleration efficiency, the solid angle under which the shock is seen by the isotropic pulsar wind, and the bow-shock geometry (Arons & Tavani 1993). It seems highly unlikely that these could produce the variability of the X-ray emission by up to two orders of magnitude observed over timescales of a few tens of seconds from PSR J1023+0038.

5.2. Accreting NS Scenario

The most immediate interpretation of the coherent X-ray pulsations observed from PSR J1023+0038 is then in terms of an accretion of at least part of the disk in-flow close to the NS magnetic poles. However, in Section 3 we already showed that assuming that the observed average X-ray luminosity L_X is entirely due to accretion onto the NS surface, the implied mass accretion rate onto the NS surface is $\dot{M}_{\rm NS} < 6 \times 10^{-13}$ $M_\odot$ yr^{-1} (see Equation (5)). According to Equation (4), and considering the value of the dipole magnetic moment of PSR J1023+0038 measured from the spin-down rate, at such a mass accretion rate the disk would be truncated beyond the light-cylinder radius. Such a large value clearly violates the criterion for accretion onto the NS surface to proceed. In order to keep the accretion disk radius closer to the corotation radius, we thus had to assume that the disk mass accretion rate was much larger than the rate at which mass is effectively accreted onto the NS, and that the excess disk mass is ejected by the system.

In addition, the simultaneous observation of a bright gamma-ray emission would be unexplained by a fully accreting scenario, considering that the transitonal pulsars PSR J1023+0038 and XSS J12270−4859 are the only LMXBs from which a *Fermi* gamma-ray counterpart could be securely identified among a population of >200 known accreting LMXBs, and this is unlikely to be the result of a selection effect. The 5σ sensitivity flux level above 100 MeV of the 3FGL *Fermi* catalog (The *Fermi*-LAT Collaboration 2015) for sources at high (low) galactic latitude[5] is in fact 2×10^{-9} cm^{-2} s^{-1} (10^{-8} cm^{-2} s^{-1}), assuming a power-law spectrum with index equal to 2. This corresponds to $\simeq 1.5 \times 10^{-12}$ erg cm^{-2} s^{-1} ($\simeq 7.5 \times 10^{-12}$ erg cm^{-2} s^{-1}). A steady 0.1–100 GeV flux like the one observed from PSR J1023+0038 in the *sub-luminous* disk state, $F = (4.6 \pm 0.6) \times 10^{-11}$ erg cm^{-2} s^{-1} (see Takata et al. 2014, and Section 2), would have been observed by *Fermi*/LAT up to $\simeq 7$ kpc (3.3 kpc if the source were at a lower latitude). On the other hand, a high-latitude low-mass X-ray binary like Cen X-4 is instead located at a distance similar to PSR J1023+0038, 1.2 kpc, and would have then been easily seen by *Fermi*/LAT, yet it has not been detected so far.

5.3. Propeller Scenario

A scenario based on a propelling NS with an accretion rate of a few $\times 10^{-11}$ $M_\odot$ yr^{-1} naturally reproduces the bolometric luminosity between few $\times 10^{34}$ erg s^{-1}, observed from transitional pulsars like PSR J1023+0038 and XSS J12270−4859 in the disk *sub-luminous* state (see Figure 1 of this paper and Figure 2 of Campana et al. 1998). We showed that we could reproduce the gamma-ray part of the SED as being due to the self-synchrotron Compton emission that originated at the turbulent boundary between a propelling magnetosphere and the disk in-flow, assuming that there is a region where electrons can be accelerated to relativistic energies. The X-ray emission is instead due to the sum of the synchrotron emission that originated from the same region and the luminosity emitted by the accretion flow. For the accretion flow luminosity not to exceed the observed X-ray luminosity, an X-ray disk radiative efficiency of less than 20% is requested.

The observed SED was reproduced by our modeling considering values of the fastness between 1.5 and 2.5, and assuming that 99% of the disk flow is ejected by the NS, and that 15% of the gravitational energy advected in the disk is available to power the propeller radiative emission. For the considered values of the fastness, the disk–magnetospheric boundary is highly magnetized ($\approx 10^6$ G; resulting from the dipolar contribution from the pulsar) to produce a synchrotron emission cutoff at energies of about 1–10 MeV. If the acceleration region is small enough it can then give a sizable SSC contribution, enough to explain the observed gamma-ray emission. Our modeling indicates that a region with a volume of $V \lesssim 10^{15}$ cm^3 is needed, corresponding to a sphere with a radius equal to $\lesssim 1$ km. Such a relatively small size could be attained if the acceleration process takes place, e.g., in filaments along the magnetic field lines at localized spots of

[5] See http://www.slac.stanford.edu/exp/glast/groups/canda/lat_Performance.htm for a plot of the sensitivity attained in four years.

the disk–magnetospheric boundary. As the volume of the emitting region decreases with decreasing ω_*, we find the higher values of ω_* considered in this work (i.e., between 2 and 2.5) more likely. For similar values of ω_*, 3D MHD simulations performed by Lii et al. (2014) showed that accretion and ejection of matter can coexist, with most of the matter being flung out by the fast rotating magnetosphere.

However, the impossibility of observationally separating contributions of the accretion flow and the propeller just at the X-ray domain is partially limiting to the model testing. This gives a larger phase space of plausible parameters for the accretion flow component, which can accommodate several different values of the fastness (see Table 1). This translates into a range of possible mass in-flow rates, between 1 and $3 \times 10^{-11}\ M_\odot\ \mathrm{yr}^{-1}$. It is also true that the more direct, testable model predictions, happen in a range of energies with no sensitive coverage (at the tens of MeV regime), or at timescales for which *Fermi*/LAT is not sensitive enough to track them (e.g., searches for correlations of gamma-ray and X-ray fluxes at the 100 s timescales cannot proceed). We also note that this model predicts no detectable TeV counterparts, which can be proven by extrapolating the predicted (or fitted) gamma-ray spectra to this domain and comparing them with the sensitivities of current or foreseen instruments (Actis et al. 2012).

A Fermi process is a possible mechanism for accelerating electrons in the magnetized, shocked environment expected at the boundary between the disk and a propelling magnetosphere (Bednarek 2009; Papitto et al. 2012; Torres et al. 2012). In P14, we assumed that a first-order process injected energy in the electron distribution at a rate

$$\ell_{\rm acc} = 1.4 \times 10^5 \xi_{0.01}\ \bar{B}_6 \mathrm{erg\ s}^{-1}, \tag{22}$$

where $\xi_{0.01}$ is the acceleration parameter in units of 0.01, and $\bar{B}_6$ is the strength of the magnetic field at the interface $\bar{B}$, in units of 10^6 G. In P14 we showed that the most efficient radiative processes at the boundary between an accretion disk and the propelling magnetosphere of a millisecond pulsar are synchrotron interaction of the accelerated electrons with the NS field lines and Compton up-scattering of the synchrotron photons by the same population of relativistic charges. Synchrotron losses proceed at a rate

$$\ell_{\rm syn} = 1.1 \times 10^5\ \bar{B}_6^2\ \gamma_4^2\ \mathrm{erg\ s}^{-1}, \tag{23}$$

where γ_4 is the maximum electron energy $\gamma_{\rm max}$ in units of 10^4, while we assume SSC losses to be $\ell_{\rm SSC} = (f-1)\ell_{\rm syn}$, where f is implicitely defined as the ratio between the total luminosity $(\ell_{\rm syn} + \ell_{\rm SSC})$ and the synchrotron luminosity $\ell_{\rm syn}$. Equating these radiative losses to the energy input of the Fermi process of electron acceleration (Equation (22)) yields the maximum electron energy

$$\gamma_{\rm max} = 8.2 \times 10^3\ f_2^{-1/2}\ \xi_{0.01}^{1/2}\ \bar{B}_6^{-1/2}, \tag{24}$$

where f_2 is the ratio between the total (synchrotron+SSC) and the synchrotron luminosity f, in units of 2. The observed high-energy cutoff of the observed SED indicates $\gamma_{\rm max} = 10^4$, and the values of f and $\bar{B}$ of our modeling (see Table 1) indicate that the previous relation is satisfied for an acceleration parameter ξ ranging from 0.03 to 0.1.

Reconnection of magnetic lines twisted in the turbulent region could also provide accelerated particles. In the case of a white dwarf propeller, such possibilities were studied by Meintjes & de Jager (2000) for the case of AE Aqr.

According to our model, a relatively strong magnetic torque is needed to power a propeller emission of $\simeq 2.5 \times 10^{34}$ erg s^{-1}, i.e., of the order of that observed in X-rays and gamma-rays from a system like PSR J1023+0038 in the *sub-luminous* disk state. For $\omega_* = 2.5$, the torque expressed by Equation (17) corresponds to an expected spin-down rate, $\dot{\nu} = N_{\rm mag}/2\pi I \simeq -4 \times 10^{-15}$ Hz s^{-1}, where an NS moment of inertia $I = 10^{45}$ g cm^2 was assumed. Lower values of the fastness give a larger expected spin-down rate. If the system is in a propeller state, a $\dot{\nu}$ larger by more than a factor of 2 with respect to that observed when the system is observed as a radio pulsar ($\dot{\nu}_{\rm dip} = -1.9 \times 10^{-15}$ Hz s^{-1}, Archibald et al. 2013) is then expected. The spin evolution during the disk state can be estimated by following the variations of the spin frequency measured from X-ray pulsations emitted in such a state and/or by a comparison with the frequency of radio pulsations that will be observed when the rotation-powered pulsar will be back on. Such a measure will then allow us to estimate the torque acting onto the NS and test our assumption that the system lies in a propeller state when it has a disk.

The variability of the X-ray emission over timescales of few tens of seconds is a characteristic feature of millisecond pulsars in the disk *sub-luminous* state. In the context of the propeller model we propose, it can be attributed to variations of the mass in-flow rate (see Equation (17)) and the related response of the fastness and of the location of the inner disk radius (Equation (4)). The observed variability timescales are indeed compatible with the viscous timescales in the inner parts of an accretion disk, as noted by Patruno et al. (2014). However, the lack of information on the possible correlation between X-ray and gamma-ray emission on timescales of few hundreds of seconds prevents us from modeling the variability of the SED, as it was done for the average SED. Linares et al. (2014) and Patruno et al. (2014) argued that at the lowest X-ray luminosity observed in the case of M28I and PSR J1023+0038, respectively, $L_X \simeq 5 \times 10^{32}$ erg s^{-1}, the inner disk radius could expand beyond the corotation surface and a radio pulsar turn-on. Even in this case, the same energy budget-based considerations made in Section 5.2 suggest that we should exclude a scenario in which the observed gamma-rays are only due to intervals during which a rotation-powered pulsar is turned on. Tendulkar et al. (2014) showed that 1023 spends less than 25% of the time in the low/dipping state; if gamma-rays are only produced in this state a 0.1–100 GeV luminosity equal to four times the observed one (i.e., $\approx 4 \times 10^{34}$ erg s^{-1}) would be implied. This would require a conversion efficiency of spin-down power into gamma-rays of 90%, not taking into account the emission not falling into the LAT energy band.

Also the bright, flat-spectrum radio emission observed from transitional millisecond pulsars in the *sub-luminous* disk state (Hill et al. 2011; Deller et al. 2014) can be taken as an indication of synchrotron emission originating from an outflow from the system. As we already noted in P14, the properties of the emitting region where we assumed that the high-energy emission originate are such that synchrotron emission would be self-absorbed. The observed radio emission should then be produced by a wider, optically thinner region such as a compact jet.

The necessity that a pulsar in a LMXB passes through a propeller regime when the mass accretion rate decreases was already identified decades ago (Illarionov & Sunyaev 1975) and reproduced by magneto-hydrodynamical simulation

(Romanova et al. 2014 and references therein). However, observational evidence has been limited and indirect, among which the rapid decrease of the X-ray emission at the end of X-ray outbursts of Aql X-1 (Campana et al. 1998, 2014), accompanied by a hardening of the X-ray spectral shape (Zhang et al. 1998), is probably the most remarkable. *Transitional* millisecond pulsars have proven to be exceptional laboratories for studying not only the evolutionary link between radio and X-ray millisecond pulsars, but also the centrifugal inhibition of accretion. During its 2013 outburst IGR J18245−2452 showed marked flux and spectral variability that were interpreted by Ferrigno et al. (2014) as products of the onset of propeller reduction of the mass in-flow. Furthermore, we showed how the *sub-luminous* disk state of PSR J1023 +0038 can be naturally interpreted with a propeller scenario, similar to the case of XSS J12270−4859 (Papitto et al. 2014). Future observations will be fundamental for detecting direct evidence of out-flowing plasma, such as spectral lines and a possible correlation between the radio and X-ray emission. Also, such observations will be used to extend knowledge of the SED and possibly detect an excess of emission with respect to the spin-down power, which would rule out a rotation-powered pulsar interpretation.

We acknowledge support from the the grants AYA2012-39303 and SGR 2014-1073. A.P. is supported by a Juan de la Cierva fellowship. D.F.T. further acknowledges the National Natural Science Foundation of China via NSFC-11473027 and the Chinese Academy of Sciences visiting professorship program 2013-T2J0007. We thank L. Burderi, E. de Oña Wilhelmi, T. Di Salvo, J. Li, N. Rea, and M. Romanova for useful discussions and comments. We acknowledge the International Space Science Institute (ISSI), which funded and hosted an international team devoted to the study of transitional millisecond pulsars, and we thank all the members of the team for fruitful discussions. We thank the anonymous referee for useful comments and suggestions.

REFERENCES

Abdo, A. A., Ajello, M., Allafort, A., et al. 2013, ApJS, 208, 17
Actis, E. V., Huang, D., Márquez, R., et al. 2012, in IAU Joint Discussion 7, IAU Joint Discussion, SLR and GPS Spatial Techniques in ITRF (Cambridge: Cambridge Univ. Press), 28P
Alpar, M. A., Cheng, A. F., Ruderman, M. A., & Shaham, J. 1982, Natur, 300, 728
Archibald, A. M., Bogdanov, S., & Patruno, A. 2014, ApJ, in press, arXiv:1412.1306
Archibald, A. M., Kaspi, V. M., Bogdanov, S., et al. 2010, ApJ, 722, 88
Archibald, A. M., Kaspi, V. M., Hessels, J. W. T., et al. 2013, arXiv:1311.5161
Archibald, A. M., Stairs, I. H., Ransom, S. M., et al. 2009, Sci, 324, 1411
Armas Padilla, M., Degenaar, N., & Wijnands, R. 2013a, MNRAS, 434, 1586
Armas Padilla, M., Wijnands, R., & Degenaar, N. 2013b, MNRAS, 436, L89
Arons, J., & Tavani, M. 1993, ApJ, 403, 249
Bassa, C. G., Patruno, A., Hessels, J. W. T., et al. 2014, MNRAS, 441, 1825
Bednarek, W. 2009, MNRAS, 397, 1420
Bernardini, F., Cackett, E. M., Brown, E. F., et al. 2013, MNRAS, 436, 2465
Bisnovatyi-Kogan, G. S., & Komberg, B. V. 1974, SvA, 18, 217
Bogdanov, S., Archibald, A. M., Bassa, C., et al. 2014, ApJ, in press, arXiv:1412.5145
Bogdanov, S., Archibald, A. M., Hessels, J. W. T., et al. 2011, ApJ, 742, 97
Bogdanov, S., & Halpern, J. P. 2015, ApJL, 803, L27
Bogdanov, S., Patruno, A., Archibald, A. M., et al. 2014, ApJ, 789, 40
Bozzo, E., Stella, L., Vietri, M., & Ghosh, P. 2009, A&A, 493, 809
Burderi, L., Possenti, A., D'Antona, F., et al. 2001, ApJL, 560, L71
Cackett, E. M., Fridriksson, J. K., Homan, J., Miller, J. M., & Wijnands, R. 2011, MNRAS, 414, 3006
Campana, S., Brivio, F., Degenaar, N., et al. 2014, MNRAS, 441, 1984
Campana, S., Colpi, M., Mereghetti, S., Stella, L., & Tavani, M. 1998, A&ARv, 8, 279
Campana, S., & Stella, L. 2003, ApJ, 597, 474
Campana, S., Stella, L., Mereghetti, S., et al. 1998, ApJL, 499, L65
Casella, P., Altamirano, D., Patruno, A., Wijnands, R., & van der Klis, M. 2008, ApJL, 674, L41
Chakrabarty, D., Tomsick, J. A., Grefenstette, B. W., et al. 2014, ApJ, 797, 92
Coti Zelati, F., Campana, S., D'Avanzo, P., & Melandri, A. 2014, MNRAS, 438, 2634
D'Angelo, C. R., & Spruit, H. C. 2010, MNRAS, 406, 1208
de Cea del Pozo, E., Torres, D. F., & Rodriguez Marrero, A. Y. 2009, ApJ, 698, 1054
Deller, A. T., Archibald, A. M., Brisken, W. F., et al. 2012, ApJL, 756, L25
Deller, A. T., Moldón, J., Miller-Jones, J. C. A., et al. 2014, arXiv:1412.5155
De Martino, D., Belloni, T., Falanga, M., et al. 2013, A&A, 550, A89
de Martino, D., Casares, J., Mason, E., et al. 2014, MNRAS, 444, 3004
De Martino, D., Falanga, M., Bonnet-Bidaud, J.-M., et al. 2010, A&A, 515, A25
Degenaar, N., & Wijnands, R. 2012, MNRAS, 422, 581
Degenaar, N., Wijnands, R., Reynolds, M. T., et al. 2014, ApJ, 792, 109
Dubus, G. 2006, A&A, 456, 801
Ekşi, K. Y., & Alpar, M. A. 2005, ApJ, 620, 390
Ekşi, K. Y., Hernquist, L., & Narayan, R. 2005, ApJL, 623, L41
Ferrigno, C., Bozzo, E., Papitto, A., et al. 2014, A&A, 567, A77
Ghosh, P. 2007, Rotation and Accretion Powered Pulsars (Singapore: World Scientific)
Ghosh, P., & Lamb, F. K. 1979, ApJ, 234, 296
Ghosh, P., Pethick, C. J., & Lamb, F. K. 1977, ApJ, 217, 578
Halpern, J. P., Gaidos, E., Sheffield, A., Price-Whelan, A. M., & Bogdanov, S. 2013, ATel, 5514, 1
Hermsen, W., Hessels, J. W. T., Kuiper, L., et al. 2013, Sci, 339, 436
Hill, A. B., Szostek, A., Corbel, S., et al. 2011, MNRAS, 415, 235
Illarionov, A. F., & Sunyaev, R. A. 1975, A&A, 39, 185
Li, K. L., Kong, A. K. H., Takata, J., et al. 2014, ApJL, 797, L111
Lii, P. S., Romanova, M. M., Ustyugova, G. V., Koldoba, A. V., & Lovelace, R. V. E. 2014, MNRAS, 441, 86
Linares, M., Bahramian, A., & Heinke, C. 2014, MNRAS, 438, 251
Lipunov, V. M. 1987, Ap&SS, 132, 1
Martín, J., Torres, D. F., & Rea, N. 2012, MNRAS, 427, 415
Meintjes, P. J., & de Jager, O. C. 2000, MNRAS, 311, 611
Nolan, P. L., Abdo, A. A., Ackermann, M., et al. 2012, ApJS, 199, 31
Pallanca, C., Dalessandro, E., Ferraro, F. R., Lanzoni, B., & Beccari, G. 2013, ApJ, 773, 122
Papitto, A., de Martino, D., & Belloni, T. M. 2015, MNRAS, 449, L26
Papitto, A., Ferrigno, C., Bozzo, E., et al. 2013, Natur, 501, 517
Papitto, A., Torres, D. F., & Li, J. 2014, MNRAS, 438, 2105
Papitto, A., Torres, D. F., & Rea, N. 2012, ApJ, 756, 188
Patruno, A., Archibald, A. M., Hessels, J. W. T., et al. 2014, ApJL, 781, L3
Patruno, A., & Watts, A. L. 2012, arXiv:1206.2727
Possenti, A., Cerutti, R., Colpi, M., & Mereghetti, S. 2002, A&A, 387, 993
Radhakrishnan, V., & Srinivasan, G. 1982, CSci, 51, 1096
Reynolds, M. T., Miller, J. M., Homan, J., & Miniutti, G. 2010, ApJ, 709, 358
Romanova, M. M., Lovelace, R. V. E., Bachetti, M., et al. 2014, in European Physical Journal Web of Conf. 64, MHD Simulations of Magnetospheric Accretion, Ejection and Plasma-field Interaction, 05001
Roy, J., Ray, P. S., Bhattacharyya, B., et al. 2015, ApJL, 800, L12
Rutledge, R. E., Bildsten, L., Brown, E. F., Pavlov, G. G., & Zavlin, V. E. 2001, ApJ, 551, 921
Saitou, K., Tsujimoto, M., Ebisawa, K., & Ishida, M. 2009, PASJ, 61, L13
Shvartsman, V. F. 1970, SvA, 14, 527
Sierpowska-Bartosik, A., & Torres, D. F. 2008, APh, 30, 239
Spitkovsky, A. 2006, ApJL, 648, L51
Spruit, H. C., & Taam, R. E. 1993, ApJ, 402, 593
Stappers, B. W., Archibald, A. M., Hessels, J. W. T., et al. 2014, ApJ, 790, 39
Strader, J., Chomiuk, L., Sonbas, E., et al. 2014, ApJL, 788, L27
Takata, J., Li, K. L., Leung, G. C. K., et al. 2014, ApJ, 785, 131
Tendulkar, S. P., Yang, C., An, H., et al. 2014, ApJ, 791, 77
The *Fermi-LAT* Collaboration 2015, ApJS, in press, arXiv:1501.02003
Torres, D. F. 2004, ApJ, 617, 966
Torres, D. F., Rea, N., Esposito, P., Li, J., Chen, Y., et al. 2012, ApJ, 744, 106
Vink, J., Bamba, A., & Yamazaki, R. 2011, ApJ, 727, 131
Wang, Y.-M. 1996, ApJL, 465, L111
Wang, Z., Archibald, A. M., Thorstensen, J. R., et al. 2009, ApJ, 703, 2017
Wijnands, R., & Degenaar, N. 2013, MNRAS, 434, 1599
Wijnands, R., & van der Klis, M. 1998, Natur, 394, 344
Zavlin, V. E. 2007, Ap&SS, 308, 297
Zhang, S. N., Yu, W., & Zhang, W. 1998, ApJL, 494, L71